FULL PAPER

Nitrogen-Doped Single-Walled Carbon Nanotubes Grown on Substrates: Evidence for Framework Doping and Their Enhanced Properties

*Yu Liu, Zhong Jin, Jinyong Wang, Rongli Cui, Hao Sun, Fei Peng, Li Wei, Zhenxing Wang, Xuelei Liang, Lianmao Peng, and Yan Li**

Nitrogen-doped single-walled carbon nanotubes (SWCNTs) are synthesized directly on silicon and quartz substrates through a normal chemical vapor deposition (CVD) method. Thermogravimetry mass spectrometry measurements and Raman spectroscopy give firm evidence for framework nitrogen doping. X-ray-photoelectron-spectroscopy analysis further obtains the bonding style of the nitrogen atoms in the carbon framework. The nitrogen doping significantly changes the properties of the SWCNTs. All of the tubes behave like metallic tubes in field-effect transistors. The doped nitrogen atoms introduce a stronger affinity for the SWCNTs to metal nanoparticles. Compared with pristine SWCNTs, the nitrogen-doped tubes show enhanced sensitivity and selectivity for electrochemical detection of some electrophilic species including O_2, H_2O_2, and Fe^{3+}. They also present improved electrocatalytic activity for oxygen reduction. These unique properties of the nitrogen-doped SWCNTs endow them with important potential applications in various fields.

1. Introduction

Single-walled carbon nanotubes (SWCNTs) have extraordinary electronic, optical, optoelectronic, and mechanical properties endowed by their unique structure;[1] therefore, they have been considered as a good candidates for scientific research and for applications in nanoscience and nanotechnology.[2–15] SWCNTs can be either metallic or semiconducting, depending on their structure. Semiconducting tubes have been used in field-effect transistors (FETs) and optoelectronic devices,[8–12] and metallic tubes have been used in high-frequency devices and interconnections for devices.[13–15] Therefore it is necessary to obtain SWCNTs with unitary conductivity in a controllable way. There are two main strategies for this purpose. One is selective synthesis by controlling the chemical vapor deposition (CVD) conditions;[16–19] the other is post-synthesis separation, such as density-gradient centrifugation,[20–22] DNA-assisted chromatography,[23,24] and selective reactions.[25–27] Compared to the post-synthesis separation methods, the selective-synthesis methods are obviously less destructive and more economical; therefore, they are more desirable. However, facile control of the preparation process is far from consummating.

Chemical doping has shown great success in silicon-based semiconductors. This strongly implies that the electronic properties of SWCNTs should be tailored by appropriate doping during the synthesis process; just like that which has been used in Si-based systems, nitrogen, boron, and phosphorous have been tried as dopants in SWCNTs.[28–32] Since nitrogen and boron have similar atomic sizes to carbon, it is much easier for them to be inserted into the carbon structures. Until now, most reports have been about the doping of multiwalled carbon nanotubes (MWCNTs), possibly due to their higher structure tolerance.[33] Bulk syntheses of doped SWCNTs have been performed by substitution reactions,[34] arc discharge,[35] laser ablation,[36] and chemical vapor deposition (CVD).[28,37] Xu et al. proved that B/N co-doping turns all SWCNTs to be semiconducting,[29] while other reports have confirmed that carbon nanotubes behave metallically when doped by either B or N alone.[30,31] Nevertheless, the synthesis of doped SWCNTs directly on substrates has not been successfully achieved yet. Compared to bulk synthesis, SWCNTs grown on substrates have obvious advantages. They have much fewer impurities and need no further purification. They are immediately ready for building devices. In addition, direct growth on substrates will accelerate the one-by-one characterization of doped SWCNTs.

In this paper, we present a CVD method for synthesizing nitrogen-doped SWCNTs on SiO_x/Si and quartz substrates using ethylenediamine or pyridine as both carbon and nitrogen sources. The so-produced nitrogen-doped SWCNTs on substrates are immediately ready for building various devices and performing various characterizations. This enables us to study

Y. Liu, Dr. Z. Jin, Dr. J. Wang, R. Cui, Dr. H. Sun, F. Peng, L. Wei, Prof. Y. Li
College of Chemistry and Molecular Engineering
Peking University
Beijing, 100871, P. R. China
E-mail: yanli@pku.edu.cn
Z. Wang, Prof. X. Liang, Prof. L. Peng
Department of Electronics
Peking University
Beijing, 100871, P. R. China

DOI: 10.1002/adfm.201002086

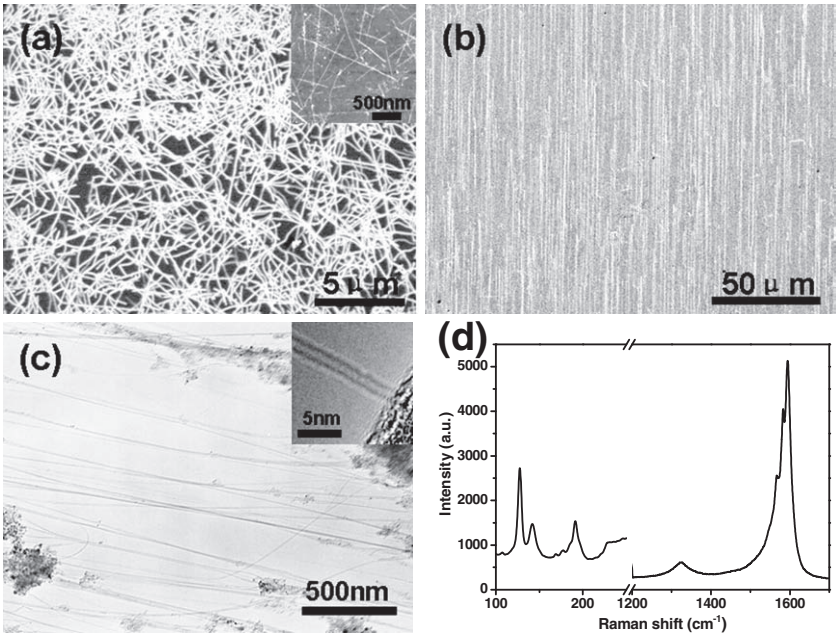

Figure 1. a) SEM image of nitrogen-doped SWCNTs on SiO_x/Si substrate; the inset is a typical AFM image of the same sample. b) SEM image of nitrogen-doped SWCNTs on quartz substrates. c) TEM and HR-TEM (inset) images of the nitrogen-doped SWCNTs, prepared using the semi-bulk method. d) A typical Raman spectrum of the nitrogen-doped SWCNTs.

the intrinsic properties of nitrogen-doped SWCNTs in situ. The nitrogen doping makes the SWCNTs all metallic, and the surface properties are also modified. They show enhanced sensitivity and selectivity for the detection of some species, such as oxygen, hydrogen peroxide, and Fe^{3+}. They also exhibit catalytic activity for the electrochemical reduction of oxygen.

In previous studies, X-ray photoelectron spectroscopy (XPS) and electron energy loss spectroscopy (EELS) have been used to determine the chemical doping of SWCNTs.[29,38] However, neither technique gives firm evidence for framework doping of SWCNTs. Here, besides XPS, we first use thermogravimetry-mass spectrometry (TG-MS) analysis to verify the skeleton doping of nitrogen in SWCNTs. TG-MS appears to be a more-effective technique for obtaining solid evidence for distinct framework doping and surface adsorption.

2. Results and Discussion

2.1. The Growth of SWCNTs with a Nitrogen-Containing Carbon Source

Using ethylenediamine as a carbon source, high-density SWCNT random networks were prepared on SiO_x/Si substrates and parallel SWCNT arrays were obtained on ST-cut quartz substrates, as shown in the scanning electron microscopy (SEM) images in **Figure 1**a,b. Most of the tubes have diameters smaller than 2 nm according to the atomic force microscopy (AFM) measurements (inset in Figure 1a), indicating they are mainly single walled. The amount of the carbon source introduced into the reactor depends greatly on the temperature of the ethylenediamine liquid because the vapor pressure of ethylenediamine is affected by the temperature. We kept the container of ethylenediamine in a constant-temperature water bath maintained at 20 °C to ensure a stable carbon stock supply. A typical transmission electron microscopy (TEM) image of the sample prepared by the semi-bulk process is shown in Figure 1c. The high-resolution TEM (HR-TEM) image given as an inset in Figure 1c clearly shows that the tube is single walled. Figure 1d presents a typical micro-Raman spectrum of the same sample as in Figure 1a at E_{laser} = 1.96 eV. Several radial-breathing-mode (RBM) peaks show up. There is a weak D band in the spectrum. The D band normally comes from defects and amorphous carbon. Nitrogen doping may introduce defects into the conjugated carbon frameworks of SWCNTs due to the different bonding forms of nitrogen to carbon. The D-band intensity of our sample is much lower than those of nitrogen-doped carbon nanotube samples reported previously. This indicates that the SWCNTs we synthesized kept their basic structural integrity, and the amorphous carbon impurities were very few.

2.2. Characterization and Evidence for Framework Nitrogen Doping of Our Samples

As stated in the introduction, the presence of nitrogen can be detected by XPS and EDX. However, it is hard to tell whether the nitrogen atoms are inserted into the carbon skeletons or just adsorb onto the surface of the carbon nanotubes. Here, we introduced TG-MS analysis to verify the nitrogen doping of our samples. As shown in **Figure 2**a, nitrogen monoxide (NO) species were detected by MS. This indicates that nitrogen was present in our samples. What is more important is that NO and CO_2 are detected spontaneously at a temperature of about 400 °C and show up together all the way to 800 °C. No nitrogen-containing species are detected at lower temperature and before the appearance of CO_2. This indicates that the nitrogen atoms do not adsorb onto the tube walls but insert into the sp^2 skeleton of carbon nanotubes. Only when the tubes are decomposed are nitrogen species released off, together with carbon species. This result presents solid evidence for the framework nitrogen doping of our samples.

Figure 2b shows the typical Raman spectra at the G-band region of the nitrogen-doped SWCNTs and pristine SWCNTs for comparison. Though the peak positions of the G^+ and G^- modes have no obvious shift, the intensity of the G^- mode is enhanced significantly by the nitrogen doping. The continuum electronic states near the Fermi level have a dynamic screening effect on longitudinal optical (LO) phonons, which leads to the appearance of a broad, asymmetric G^- mode, the Breit–Wigner–Fano (BWF) mode, in metallic SWCNTs. This BWF mode is highly dependent on the density of states (DOS) near the Fermi

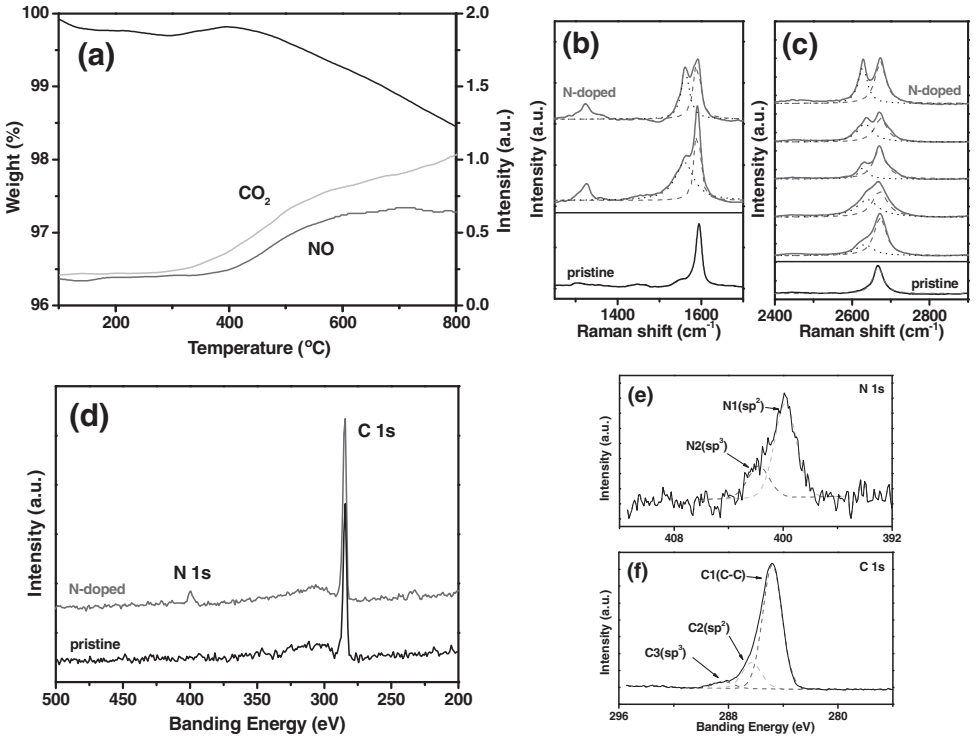

Figure 2. a) TG-MS analysis of the nitrogen-doped SWCNTs. CO_2 and NO are the decomposition products of C and N, respectively. b,c) Raman spectra of the G band and G' band of the nitrogen-doped SWCNTs on SiO_x/Si substrates at E_{laser} = 2.33 eV. The dashed and dotted lines in (b) correspond to the G^+ and G^- peaks from Lorentzian fitting; the dashed and dotted lines in (c) correspond to the G'_{pris} and G'_d peaks from Lorentzian fitting. d) XPS spectra of pristine and nitrogen-doped SWCNTs. e) XPS spectrum of N 1s of the nitrogen-doped SWCNTs. The N 1s peak can be split into two Lorentzian peaks at 399.8 and 401.8 eV. f) XPS spectrum of C 1s of the nitrogen-doped SWCNTs. The C 1s peak can be divided into three Lorentzian peaks at 284.8, 286.3, and 288.3 eV.

surface.[39,40] Nitrogen doping increases the DOS of SWCNTs, which results in an improved screening effect; thereby, a more-prominent BWF mode is observed.

The G' band in the Raman spectrum is second order. It is highly sensitive to changes in the sp^2 carbon structures.[41,42] Therefore, the G' band has been used to characterize substitutional doping in SWCNTs.[32] Figure 2c shows the Raman spectrum at the G' band region of the nitrogen-doped SWCNTs on SiO_x/Si substrates. The pristine SWCNT sample shows a single-peak G' band at 2670 cm^{-1}, while the nitrogen-doped SWCNT samples have two G' features. One (denoted as G'_{pris}) is identical to that in the pristine samples; the other band, denoted as G'_d, appears at 2630 cm^{-1}, and originates from the nitrogen doping. We examined tens of individual SWCNTs and found that G'_d bands appear in each Raman spectrum of the nitrogen-doped SWCNT samples. We also examined over 20 isolated, pristine SWCNTs and no visible G'_d bands were found. The typical G' bands of nitrogen-doped SWCNTs on SiO_x/Si substrates are shown in Figure 2c. The typical G' bands of the corresponding pristine SWCNTs are also shown for comparison.

In the XPS spectrum, the nitrogen-doped sample shows an obvious N 1s peak at about 400 eV (Figure 2d). The nitrogen content in the sample is 3 at-%. There are mainly two components in the N 1s spectrum, indicating that the N atoms have two types of bonding structure in the carbon nanotubes (Figure 2e). The peak at 399.8 eV corresponds to pyridinic nitrogen and the peak at 401.8 eV is attributed to graphitic nitrogen.[38] It can be found from the peak intensity that more nitrogen atoms are pyridinic. Three components emerge in the C 1s spectrum (Figure 2f): the main peak at 284.8 eV corresponds to graphite-like sp^2 C, indicating that most of the C atoms are not bonded with N atoms;[38] the small peaks at 286.3 and 288.3 eV correspond to nitrogen sp^2 C and sp^3 C, respectively:[38] they may originate from the nitrogen doping or the defects of the SWCNTs.

2.3. Copper Coating on Nitrogen-Doped and Pristine SWCNTs

The introduction of nitrogen into the framework may change the electron-density distribution of the SWCNTs, therefore affecting their surface properties. We studied the adsorption abilities of the pristine and nitrogen-doped SWCNTs with copper in a vacuum chamber. The two samples were placed close to each other to keep the same distance from the evaporation source. It is obvious that the Cu particles coated on the nitrogen-doped SWCNTs are much more uniform and the density is remarkably higher (**Figure 3**a,b). Theoretical and experimental reports[43–45] have proved that doped SWCNTs have a stronger interaction with transition metals compared to the pristine SWCNTs. Metal particles can hardly attach to the side walls of defect-free pure SWCNTs since there are few nucleation centers on the perfect

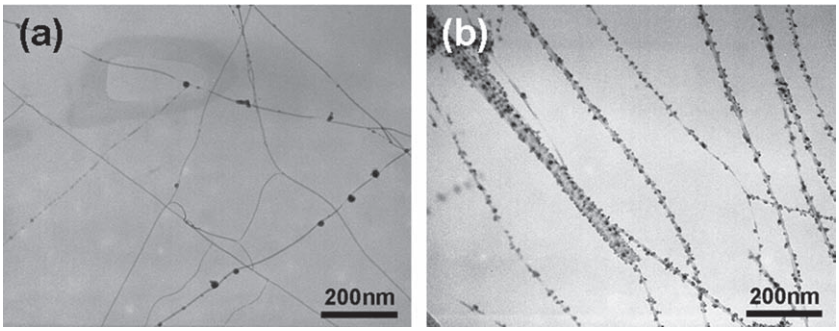

Figure 3. TEM images of Cu particles adsorbed on the sidewalls of pristine (a) and nitrogen-doped (b) SWCNTs, respectively.

carbon structures. The binding energies between nitrogen and metal atoms are higher, so these nitrogen-doped sites could act as the nucleation centers. This result further supports that the nitrogen atoms are doped uniformly into the sidewalls of SWCNTs. What we can expect futhermore is that the nitrogen-doped SWCNTs may be more appropriate for being applied in SWCNT-based inorganic composites because of their higher affinity to the inorganic matrix.

2.4. The Metallic Transport Properties of the Nitrogen-Doped SWCNTs

Terrones' group predicted theoretically that for nitrogen-doped, semiconducting SWCNTs, the electronic state created by the nitrogen doping lies beneath the conduction bands and is occupied by an extra electron.[46] The Fermi level is shifted close to the conduction bands, causing all semiconducting SWCNTs to be metallic. We get consistent results from our experiments. Multi-nanotube FET devices were fabricated to study the transport properties of the nitrogen-doped SWCNTs (**Figure 4**a,b). SWCNT random networks were used. The channel width of the FETs was 500 nm, which made most of the SWCNTs directly connect to the source and drain electrodes. Thus, a contact resistance among the SWCNTs was effectively avoided and the intrinsic electronic properties of the SWCNTs could be investigated. The densities of the pristine and nitrogen-doped samples were almost the same and 500 ± 100 tubes were laid between the electrodes in each FET device. The typical I_{ds}–V_{ds} curves are shown in Figure 4c. The pristine SWCNT sample had an on/off ratio of 2, indicating that there were 1/3 metallic SWCNTs in the device, which is the typical proportion for the normal pristine SWCNTs, while for the nitrogen-doped SWCNT sample, the conductance is twice and the modulation ability is much weaker than in the pristine sample. It shows an almost linear I_{ds}–V_{ds} behavior, which means that the proportion of metallic SWCNTs has increased remarkably. The average single-tube resistance for the nitrogen-doped SWCNTs is 10 ± 4 kΩ μm^{-1}, which is consistent with that of the pristine metallic SWCNTs at low bias voltage.[47–49] This indicates that the nitrogen doping does not introduce additional resistance to the tubes. It has been reported that defects would increase the resistance of SWCNTs greatly;[49] thus nitrogen doping does not introduce too many structural defects since the average resistance has not obviously increased. We examined 10 FET devices for each kind of SWCNTs, and the results repeated quite well.

2.5. Improved Oxygen-Detection Sensitivity of Nitrogen-Doped SWCNTs

It has been demonstrated that carbon nanotubes are sensitive materials for the detection of various gases such as H_2, NH_3, NO_2, and SO_2.[50–54] But for O_2 detection, the response signals are quite weak,[53,55] which makes it difficult for the SWCNTs to act as O_2 sensors. Nevertheless, the importing of nitrogen atoms into the framework of the SWCNTs makes the tubes more electron rich and hence might enhance the sensitivity to the highly electron-affinitive O_2. We used pristine and nitrogen-doped SWCNTs with the same density to fabricate chem-resistor sensors. This kind of sensor involves electrical contacts at the two ends of a SWCNT network film (**Figure 5**a). The signal changes originate from the charge transfer between adsorbed molecules and the valence bands of the SWCNTs. The current-change results are shown in Figure 5b. In the case of the pristine SWCNT sensor, the current increased by only 10% when the O_2 pressure approached 500 Pa, which is consistent with previous reports,[53,55] while the nitrogen-doped SWCNT sensor had a current increased by 30%, which is 3 times that of the pristine SWCNT sensor. The nitrogen-doped SWCNTs show an obvious enhanced sensibility for O_2 detection.

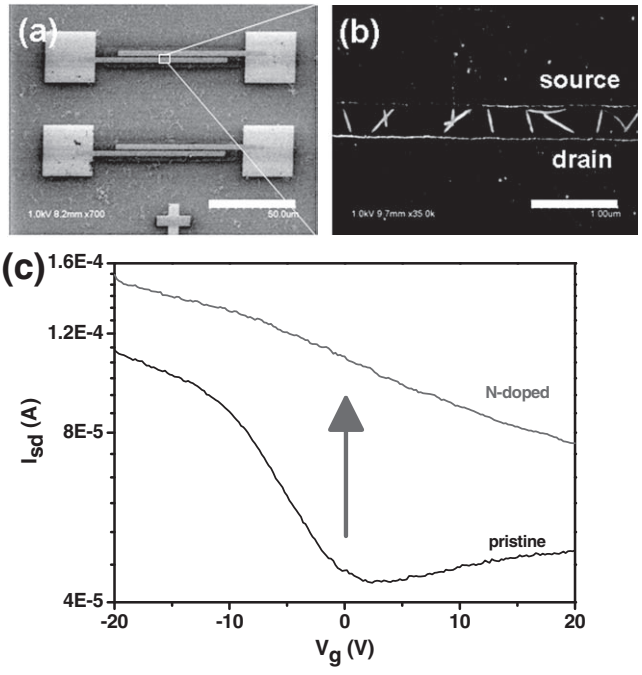

Figure 4. a) SEM image of the SWCNT-based FETs: the scale bar is 50 μm. b) A magnified image of the marked region in (a); the scale bar is 1 μm. The SWCNTs were connected to the source and drain electrodes directly. c) Typical I_{ds}–V_{ds} curves of the pristine- and nitrogen-doped-SWCNT FET devices.

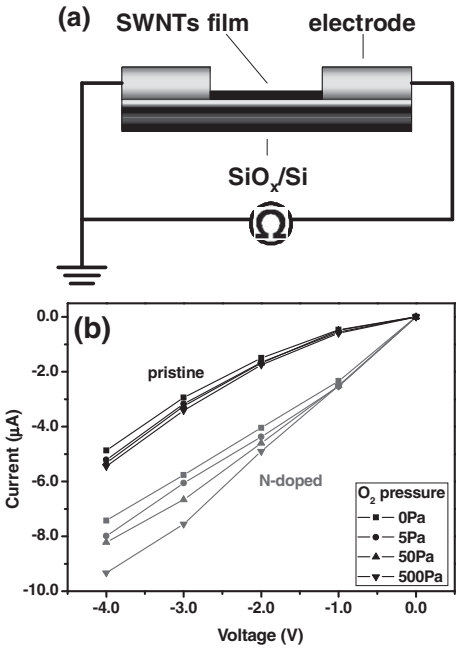

Figure 5. a) Scheme of the SWCNT-based chem-resistor sensor. b) *I–V* curves of the pristine- and nitrogen-doped-SWCNT gas sensors at various O_2 pressures (0, 5, 50, and 500 Pa).

2.6. Enhanced Electrochemical Activity by Using Nitrogen-Doped SWCNTs as Electrodes

Nitrogen-doped SWCNTs can also be used as electrode materials for electrochemical analysis.[56] Such a device is shown in **Figure 6**a. Using SWCNTs as the working electrode can lower the detection limit by lowering the background currents.[56] However, the selectivity and the sensitivity of the device are not satisfying, since the side walls of SWCNTs are chemically stable with few defect sites.[56] Our nitrogen-doped SWCNT samples may be more advantageous in this issue because additional active sites have been introduced into the tube side walls by nitrogen doping. We used both pristine and nitrogen-doped SWCNTs of similar density to fabricate this kind of device. Cyclic voltammetry (CV) measurement results for H_2O_2 and Fe^{3+} are shown in Figure 6b and c, respectively. For the H_2O_2 detection, the oxidation-current difference is obvious between the two samples of different concentration (5×10^{-6} M and 20×10^{-6} M, respectively). The signal intensity of the nitrogen-doped sensor is twice that of the pristine-SWCNT sensor. The pristine-SWCNT sensor only has a slight reduction-current change compared to the background for the 5×10^{-6} M Fe^{3+} solution, which is almost indistinguishable to the blank. This indicates that 5×10^{-6} M is out of the detection limit of the pristine SWCNTs for the detection of Fe^{3+}. However, the nitrogen-doped SWCNT sensor has a detection signal significant enough for an accurate measurement.

The nitrogen doping can increase the chemical activities of SWCNTs as a result of the extra electrons from the nitrogen atoms. Moreover, the nitrogen-doping sites may have stronger interactions with some electrophilic species, such as O_2 molecules, O radicals (the intermediate product of both the oxidation of H_2O_2 and oxygen reduction), and Fe^{3+}. Therefore more electrophilic species could be adsorbed onto the sidewalls of the nitrogen-doped SWCNTs and the interaction between the adsorbed species and the SWCNTs should be stronger. Then, the electronic structure of the nitrogen-doped SWCNTs would have greater modification. For some other species, like dopamine, o-dihydroxybenzene, and $Fe(CN)_6^{3+}$, no obvious differences between the pristine and nitrogen-doped sensors have been found in our experiments. These results suggest that the nitrogen-doped SWCNTs might be more sensitive and selective than the pristine SWCNTs in electrochemical analysis.

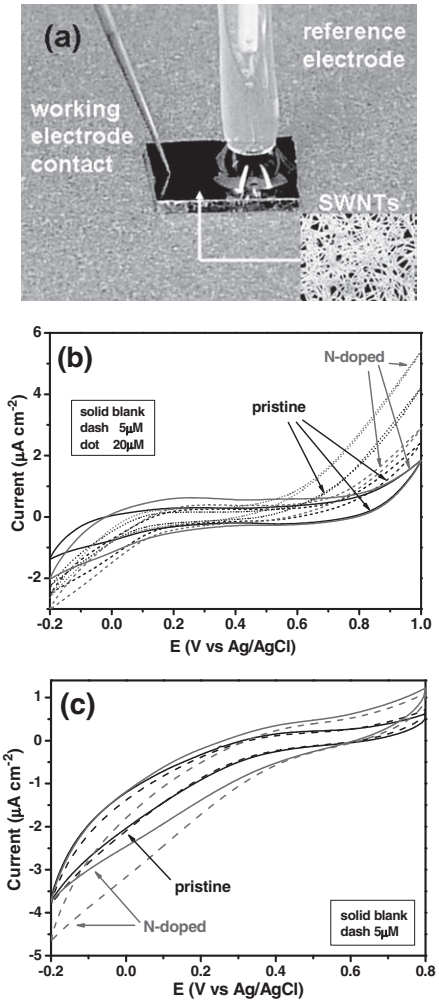

Figure 6. a) Photograph of the electrochemical sensor. b,c) The CV curves of the pristine- and nitrogen-doped-SWCNTs sensors for H_2O_2 (b) and Fe^{3+} (c) detection. The concentrations of H_2O_2 were 5×10^{-6} M (dashed line) and 20×10^{-6} M (dotted line) in phosphate buffer solution (pH = 7.4). The concentration of Fe^{3+} was 5×10^{-6} M (dashed line) in 0.1 M HCl solution. The backgrounds were recorded in 0.1 M KCl. The scan rate was 100 mV s^{-1}.

Recently, nitrogen-doped CNTs have been found to have a high electrocatalytic activity for oxygen reduction, which could replace Pt-based electrocatalysts in fuel cells.[57] We also investigated the electrocatalytic activity of our nitrogen-doped SWCNTs for oxygen reduction using a similar installation to that in Figure 6a. The result is shown in **Figure 7**. Compared to the

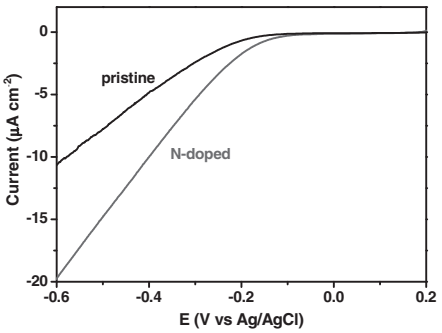

Figure 7. The voltammograms of the pristine and nitrogen-doped SWCNTs for oxygen reduction in 0.1 M KOH.

pristine SWCNTs, nitrogen-doped samples increased the reduction potential by 50 mV and doubled the reduction current.

3. Conclusions

We systematically studied the preparation, characterization, and properties of nitrogen-doped SWCNTs on substrates. Firstly, we developed a CVD method to synthesize nitrogen-doped SWCNTs directly on SiO_x/Si and quartz substrates using nitrogen-containing carbon stocks. Secondly, we obtained a decisive characterization of the nitrogen doping. TG-MS was first used to verify that the nitrogen was doped into the tube frameworks. Raman spectroscopy gave additional evidence for this argument. XPS results showed that the nitrogen atoms were mainly bonded into the carbon frameworks in the pyridinic form, and that graphitic nitrogen atoms also exist. Thirdly, we made careful comparison of the properties of nitrogen-doped and pristine SWCNTs and demonstrated the superior performance of nitrogen-doped SWCNTs. Nitrogen doping made the SWCNTs become all metallic. This is important for obtaining SWCNTs of homogeneous properties for further applications. The nitrogen doping introduced nucleation centers and anchor spots for metal nanoparticles. Therefore, it was much easier for copper to be coated on the nitrogen-doped SWCNTs. This might be helpful for applications in SWCNT-based inorganic composites. The extra electrons from the N atoms made the nitrogen-doped SWCNTs have stronger interactions with some electrophilic species, such as O_2 molecules, O radicals, and Fe^{3+}. This effect enhances the sensitivity and the selectivity of SWCNT-based chemical sensors. Nitrogen-doped SWCNTs also showed an electrocatalytic activity to the oxygen-reduction reaction. All of these results show that the nitrogen-doped SWCNTs present excellent properties and may find applications as conducting, composite, sensing, and catalytic materials with enhanced performance.

4. Experimental Section

Growth of Nitrogen-Doped SWCNTs: Typically, $FeCl_3$/EtOH solution (2 μL, 1 mmol L^{-1}) was dropped onto the SiO_x/Si or ST-cut quartz substrates to actas the catalyst precursor. The substrates were heated to 700 °C in a horizontal quartz tube (25 mm in diameter) and kept for 5 min to oxidize the $FeCl_3$. Then, the heating temperature was elevated to 880 °C under an Ar flow (400 sccm). Subsequently, the Ar was shut off and a H2 flow (100 sccm) was introduced into the system, passing a steel tank containing ethylenediamine or pyridine, which was held at 20 °C using a constant-temperature water bath. After 15 min, the quartz tube was cooled down to room temperature under Ar. We also performed semi-bulk preparation of nitrogen-doped SWCNTs. Instead of the $FeCl_3$/EtOH solution, a $FeCl_3$ precursor supported on Al_2O_3 powder[58] was spread on the SiO_x/Si substrates, and nitrogen-doped SWCNTs were then grown in an identical procedure and CVD conditions. The pristine SWCNTs were synthesized using ethanol as the carbon source.

Characterization and Doping Analysis: A Hitachi S4800 scanning electron microscope was used with an acceleration voltage of 1 kV to take the SEM images. AFM images were taken using a Seiko SPA400 SPM. The Raman spectra were collected using a HORIBA Jobin Yvon LabRam ARAMIS Raman spectrometer with excitation energies of 1.96 eV and 2.33 eV, using a 100× air objective. The laser energy was carefully controlled to avoid any heat effects. A NETZSCH STA449C/Qms 403C instrument was used to obtain the TG-MS data: the samples were heated at a rate of 5 °C min^{-1} under Ar protection. The XPS data were collected using an AXIS-Ultra instrument from Kratos Analytical. The TEM images were taken using a JEM-200CX TEM and the HR-TEM images were obtained using a Hitachi 9000 TEM. The accelerating voltages were both 100 kV. For the experiments of copper coating on the SWCNTs, the pristine and nitrogen-doped SWCNTs were placed adjacent in a vacuum (10–3 Pa) chamber at a distance of 15 cm from the evaporation source. Cu powder (1 mg) was evaporated.

Fabrication and Measurement of the Devices: The substrates with the SWCNT networks upon them were directly used to fabricate the FET devices. The source and drain electrodes were deposited by electron-beam lithography. The channel distance was 500 nm to avoid a contact effect from the SWCNTs. The measurements were taken using a Keithley 4200 semiconductor characterization system. The SWCNTs not in the channels were removed by reactive ion etching (RIE) in oxygen plasma. The bias voltage was 1 mV.

Two Au electrodes were deposited on the SWCNTs network films to form resistor gas sensors. A Keithley 2400 digital sourcemeter was used to detect the current changes. The devices were put into vacuum (10–3 Pa) for 48 h before detection to remove the adsorbed O_2.

The electrochemical sensors used the SWCNT network as the working electrode on a SiO_x/Si substrate. A Au film was deposited on part of the substrate as the working electrode contact. A drop of solution (5 μL, contact area 3 mm in diameter) was placed on the SWCNT network close to the Au film but avoiding contact and a micro reference electrode (Ag/AgCl) was inserted into the solution drop. The CV measurements were taken using a CHI660C electrochemistry workstation (Shanghai Chenhua). The detection of H_2O_2 was performed in a phosphate buffer solution of pH = 7.4 and the detection of Fe^{3+} was in HCl solution (0.1 mol L^{-1}). The oxygen-reduction reaction was carried out in 0.1 M KOH solution. Before all of the electrochemical experiments, both the pristine and nitrogen-doped SWCNT sensors were purified by electrochemical oxidation in a phosphate buffer solution (pH = 6.8) at a potential of 1.7 V (vs Ag/AgCl) for 5 min to passivate the Fe residues present in the samples.

Acknowledgements

Y.L. and Z.J. contributed equally to this research. The authors thank funding support from the Ministry of Science and Technology of China (Projects 2011CB933003 and 2007CB936202) and the National Natural Science Foundation of China (Project 50772002).

Received: October 4, 2010
Revised: November 5, 2010
Published online: January 19, 2011

[1] R. D. Saito, G.; M. S. Dresselhaus, in *Physical Properties of Carbon Nanotubes*, Imperial College Press, London, the United Kindom **1998**.
[2] S. Saito, *Science* **1997**, *278*, 77.
[3] S. J. Tans, A. R. M. Verschueren, C. Dekker, *Nature* **1998**, *393*, 49.
[4] P. Avouris, T. Hertel, R. Martel, T. Schmidt, H. R. Shea, R. E. Walkup, *Appl. Surf. Sci.* **1999**, *141*, 201.
[5] T. Rueckes, K. Kim, E. Joselevich, G. Y. Tseng, C. L. Cheung, C. M. Lieber, *Science* **2000**, *289*, 94.
[6] H. J. Dai, *Surf. Sci.* **2002**, *500*, 218.
[7] O. Zhou, H. Shimoda, B. Gao, S. J. Oh, L. Fleming, G. Z. Yue, *Acc. Chem. Res.* **2002**, *35*, 1045.
[8] P. Avouris, Z. Chen, V. Perebeinos, *Nat. Nanotechnol.* **2007**, *2*, 605.
[9] M. E. Itkis, A. P. Yu, R. C. Haddon, *Nano Lett.* **2008**, *8*, 2224.
[10] L. Ding, S. Wang, Z. Zhang, Q. Zeng, Z. Wang, T. Pei, L. Yang, X. Liang, J. Shen, Q. Chen, R. Cui, Y. Li, L.-M. Peng, *Nano Lett.* **2009**, *9*, 4209.
[11] N. M. Gabor, Z. H. Zhong, K. Bosnick, J. Park, P. L. McEuen, *Science* **2009**, *325*, 1367.
[12] T. Mueller, M. Kinoshita, M. Steiner, V. Perebeinos, A. A. Bol, D. B. Farmer, P. Avouris, *Nat. Nanotechnol.* **2009**, *5*, 27.
[13] M. S. Tahvili, S. Jahanmiri, M. H. Sheikhi, *Int. J. Numer. Modelling: Electron. Networks, Devices Fields.* **2009**, *22*, 369.
[14] Y. Chai, Z. Y. Xiao, P. C. H. Chan, *Nanotechnology* **2010**, *21*.
[15] H. Li, C. A. Xu, K. Banerjee, *IEEE Design Test Comput.* **2010**, *27*, 20.
[16] S. M. Bachilo, L. Balzano, J. E. Herrera, F. Pompeo, D. E. Resasco, R. B. Weisman, *J. Am. Chem. Soc.* **2003**, *125*, 11186.
[17] X. L. Li, X. M. Tu, S. Zaric, K. Welsher, W. S. Seo, W. Zhao, H. J. Dai, *J. Am. Chem. Soc.* **2007**, *129*, 15770.
[18] B. Wang, C. H. P. Poa, L. Wei, L. J. Li, Y. H. Yang, Y. Chen, *J. Am. Chem. Soc.* **2007**, *129*, 9014.
[19] L. Ding, A. Tselev, J. Y. Wang, D. N. Yuan, H. B. Chu, T. P. McNicholas, Y. Li, J. Liu, *Nano Lett.* **2009**, *9*, 800.
[20] Z. H. Chen, X. Du, M. H. Du, C. D. Rancken, H. P. Cheng, A. G. Rinzler, *Nano Lett.* **2003**, *3*, 1245.
[21] Y. Maeda, S. Kimura, M. Kanda, Y. Hirashima, T. Hasegawa, T. Wakahara, Y. F. Lian, T. Nakahodo, T. Tsuchiya, T. Akasaka, J. Lu, X. W. Zhang, Z. X. Gao, Y. P. Yu, S. Nagase, S. Kazaoui, N. Minami, T. Shimizu, H. Tokumoto, R. Saito, *J. Am. Chem. Soc.* **2005**, *127*, 10287.
[22] A. A. Green, M. C. Hersam, *Nano Lett.* **2008**, *8*, 1417.
[23] M. Zheng, A. Jagota, E. D. Semke, B. A. Diner, R. S. McLean, S. R. Lustig, R. E. Richardson, N. G. Tassi, *Nat. Mater.* **2003**, *2*, 338.
[24] M. Zheng, A. Jagota, M. S. Strano, A. P. Santos, P. Barone, S. G. Chou, B. A. Diner, M. S. Dresselhaus, R. S. McLean, G. B. Onoa, G. G. Samsonidze, E. D. Semke, M. Usrey, D. J. Walls, *Science* **2003**, *302*, 1545.
[25] D. Chattopadhyay, L. Galeska, F. Papadimitrakopoulos, *J. Am. Chem. Soc.* **2003**, *125*, 3370.
[26] M. S. Strano, C. A. Dyke, M. L. Usrey, P. W. Barone, M. J. Allen, H. W. Shan, C. Kittrell, R. H. Hauge, J. M. Tour, R. E. Smalley, *Science* **2003**, *301*, 1519.
[27] C. Menard-Moyon, N. Izard, E. Doris, C. Mioskowski, *J. Am. Chem. Soc.* **2006**, *128*, 6552.
[28] W. L. Wang, X. D. Bai, E. G. Wang, *Int. J. Nanosci.* **2007**, *6*, 431.
[29] Z. Xu, W. G. Lu, W. L. Wang, C. Z. Gu, K. H. Liu, X. D. Bai, E. G. Wang, H. J. Dai, *Adv. Mater.* **2008**, *20*, 3615.
[30] W. K. Hsu, S. Y. Chu, E. Munoz-Picone, J. L. Boldu, S. Firth, P. Franchi, B. P. Roberts, A. Schilder, H. Terrones, N. Grobert, Y. Q. Zhu, M. Terrones, M. E. McHenry, H. W. Kroto, D. R. M. Walton, *Chem. Phys. Lett.* **2000**, *323*, 572.
[31] M. Terrones, P. M. Ajayan, F. Banhart, X. Blase, D. L. Carroll, J. C. Charlier, R. Czerw, B. Foley, N. Grobert, R. Kamalakaran, P. Kohler-Redlich, M. Ruhle, T. Seeger, H. Terrones, *Appl. Phys. A: Mater. Sci. Process.* **2002**, *74*, 355.
[32] I. O. Maciel, J. Campos-Delgado, E. Cruz-Silva, M. A. Pimenta, B. G. Sumpter, V. Meunier, F. Lopez-Urias, E. Munoz-Sandoval, H. Terrones, M. Terrones, A. Jorio, *Nano Lett.* **2009**, *9*, 2267.
[33] K. Xiao, Y. Liu, P. A. Hu, G. Yu, Y. Sun, D. Zhu, *J. Am. Chem. Soc.* **2005**, *127*, 8614.
[34] D. Golberg, Y. Bando, W. Han, K. Kurashima, T. Sato, *Chem. Phys. Lett.* **1999**, *308*, 337.
[35] L. J. Li, M. Glerup, A. N. Khlobystov, J. G. Wiltshire, J. L. Sauvajol, R. A. Tavlor, R. J. Nicholas, *Carbon* **2006**, *44*, 2752.
[36] P. L. Gai, O. Stephan, K. McGuire, A. M. Rao, M. S. Dresselhaus, G. Dresselhaus, C. Colliex, *J. Mater. Chem.* **2004**, *14*, 669.
[37] W. L. Wang, X. D. Bai, K. H. Liu, Z. Xu, D. Golberg, Y. Bando, E. G. Wang, *J. Am. Chem. Soc.* **2006**, *128*, 6530.
[39] S. D. M. Brown, A. Jorio, P. Corio, M. S. Dresselhaus, G. Dresselhaus, R. Saito, K. Kneipp, *Phys. Rev. B: Condens. Matter* **2001**, *63*, 155414.
[40] M. Fouquet, H. Telg, J. Maultzsch, Y. Wu, B. Chandra, J. Hone, T. F. Heinz, C. Thomsen, *Phys. Rev. Lett.* **2009**, *102*, 075501.
[41] I. O. Maciel, N. Anderson, M. A. Pimenta, A. Hartschuh, H. H. Qian, M. Terrones, H. Terrones, J. Campos-Delgado, A. M. Rao, L. Novotny, A. Jorio, *Nat. Mater.* **2008**, *7*, 878.
[42] I. O. Maciel, M. A. Pimenta, M. Terrones, H. Terrones, J. Campos-Delgado, A. Jorio, *Phys. Status Solidi B* **2008**, *245*, 2197.
[38] C. Morant, J. Andrey, P. Prieto, D. Mendiola, J. M. Sanz, E. Elizalde, *Phys. Status Solidi A* **2006**, *203*, 1069.
[43] K. Y. Jiang, A. Eitan, L. S. Schadler, P. M. Ajayan, R. W. Siegel, N. Grobert, M. Mayne, M. Reyes-Reyes, H. Terrones, M. Terrones, *Nano Lett.* **2003**, *3*, 275.
[44] A. Zamudio, A. L. Elias, J. A. Rodriguez-Manzo, F. Lopez-Urias, G. Rodriguez-Gattorno, F. Lupo, M. Ruhle, D. J. Smith, H. Terrones, D. Diaz, M. Terrones, *Small* **2006**, *2*, 346.
[45] W. An, C. H. Turner, *J. Phys. Chem. C* **2009**, *113*, 7069.
[46] E. Cruz-Silva, F. Lopez-Urias, E. Munoz-Sandoval, B. G. Sumpter, H. Terrones, J. C. Charlier, V. Meunier, M. Terrones, *ACS Nano* **2009**, *3*, 1913.
[47] Z. Yao, C. L. Kane, C. Dekker, *Phys. Rev. Lett.* **2000**, *84*, 2941.
[48] A. Javey, J. Guo, M. Paulsson, Q. Wang, D. Mann, M. Lundstrom, H. Dai, *Phys. Rev. Lett.* **2004**, *92*, 106804.
[49] P. Sundqvist, F. J. Garcia-Vidal, F. Flores, M. Moreno-Moreno, C. Gomez-Navarro, J. S. Bunch, J. Gomez-Herrero, *Nano Lett.* **2007**, *7*, 2568.
[50] S. Chopra, A. Pham, J. Gaillard, A. Parker, A. M. Rao, *Appl. Phys. Lett.* **2002**, *80*, 4632.
[51] L. Valentini, I. Armentano, J. M. Kenny, C. Cantalini, L. Lozzi, S. Santucci, *Appl. Phys. Lett.* **2003**, *82*, 961.
[52] H. Q. Nguyen, J. S. Huh, *Sens. Actuators B* **2006**, *117*, 426.
[53] S. G. Yu, W. K. Yi, *IEEE Trans. Nanotechnol.* **2007**, *6*, 545.
[54] I. Sayago, H. Santos, M. C. Horrillo, M. Aleixandre, M. J. Fernandez, E. Terrado, I. Tacchini, R. Aroz, W. K. Maser, A. M. Benito, M. T. Martinez, J. Gutierrez, E. Munoz, *Talanta* **2008**, *77*, 758.
[55] P. G. Collins, K. Bradley, M. Ishigami, A. Zettl, *Science* **2000**, *287*, 1801.
[56] P. Bertoncello, J. P. Edgeworth, J. V. Macpherson, P. R. Unwin, *J. Am. Chem. Soc.* **2007**, *129*, 10982.
[57] K. P. Gong, F. Du, Z. H. Xia, M. Durstock, L. M. Dai, *Science* **2009**, *323*, 760.
[58] W. W. Zhou, Y. Zhang, X. M. Li, S. L. Yuan, Z. Jin, J. J. Xu, Y. Li, *J. Phys. Chem. B* **2005**, *109*, 6963.